1. Nested PCR

Target Sequence: AGTCTTCTGACCAGAGGCAG

The expected sequence of the wild-type (unedited) amplicon:

GCCAAGATCCAGGTCAGACACTTATATCTCCCAGCCTCAAGATCAGG

ATCACAGGTGAGTCTTCCAGTTCTGAGTTGTAGTTCATTCCAGACATA

GTCAGGTTGACAACCAGGCGCAGCCACTACAGGGGGTTGCATAGCAC

CACTGATGTGCCTGAGGCTCTCCTTGTCCCTGAGGCAACCAGGGCAAG

GGTTTAGAATTAAAATGCATAGCAACAGCCCAAACCGACGTTTTGGGT

CTCCATAGCCCTTAGTGACCAGTTCTGGTGATTGTCTCCTTGCAGGTTA

TCCAGGCCGTGTTCTTCGGCATCTGTGTGCTGACTGACCTCTCTAGTCT

TCTGACCAGAGGCAGCGGGAACCAGGAGCAAGAACGACAGCTCAGG

AAGCTCATCTCTCTCCGGGACTGGACGCTGGCCGTGCTGGCCTTCCCT

GTCGGGGTTGTGAGTATGAGACAGGATGTACTTAGCACAGAAGACAT

GTGGGTCCCACTTCAGATTTGGTTTTGTTTGTTTGTTTTTTTGTTTGTTTT

TTAATGAGGGCTCTTTCTAGAAGAGTTCTTCCTTTAGCTGGTACTAGGG

ACAGAACCCAGGACCTACCTCATGGCTCACCCAAGGTTTCT

First-round primers:

Aig1-nested-FP: GCCAAGATCCAGGTCAGACACT

Aig1-nested-RP: AGAAACCTTGGGTGAGCCATGA

Second-round primers:

Aig1-FP: CATAGCACCACTGATGTGCCTGA

Aig1-RP: GGTTCTGTCCCTAGTACCAGCTAA

	Template	Amplicon Size	Cycling Conditions (Annealing)
First Round	Genomic DNA	~620 bp	58°C for 35 cycles
Second Round	1st-round product	~450 bp	58°C for 35 cycles

2. Flow Cytometry antibody Pannels

Myeloid/Tex Pannel			
Antigen	Fluorophore	Conc.	Origin
CD45	APC-Cy7	400	BioLegend, 103116
F4/80	PE	400	abclonal, A25659
CD8	BV605	400	BioLegend, 100744
Tim3	BV711	400	BioLegend, 119727
PD-1	FITC	400	BioLegend, 135214
CD11b	PE-Cy7	400	BioLegend, 101216
Tim4	APC	400	BioLegend, 130008
MHC II	AF700	400	abclonal, A25999
CD11c	BV510	400	BioLegend, 117353
Ly6G	PE/Dazzle™ 594	400	BioLegend, 127648

Antibodies conjugated to PE/Dazzle™ 594 were detected in the PE-Texas Red channel.

Myeloid/Tex Pannel			
Antigen	Fluorophore	Conc.	Origin
IFN-γ	PE-Cy7	300	BioLegend, 505826
FOXP3	PE	300	abclonal, A26227
CD45	APC-Cy7	400	BioLegend, 103116
NK1.1	BV605	400	BioLegend, 108753
TCRβ	BV785	400	BioLegend, 109249
CD19	AF700	400	abclonal, A26193
TCRγ/δ	PerCP-Cy5.5	400	BioLegend, 118118

*intracellular marker

3. Immunofluorescence staining

For the co-staining of F4/80 and Tim-4, tissue sections were first incubated with a mixture of primary antibodies including anti-F4/80 (Chicken IgY, abcam, ab320060, 1:100) and Alexa Fluor 647-conjugated anti-mouse Tim-4 (BioLegend, 130008, 1:500) overnight at 4°C. After washing, sections were incubated with Donkey anti-Chicken IgY (H+L) Secondary Antibody, Alexa Fluor 488 (Invitrogen, A78948, 1:4000) for 1 h at room temperature.

For the co-staining of F4/80 and PD-L1, tissue sections were incubated with a mixture of primary antibodies including anti-F4/80 (Chicken IgY, abcam, ab320060, 1:100) and anti-PD-L1 (Rabbit pAb, ABclonal, A11273, 1:100) overnight at 4°C. After washing, sections were incubated with a mixture of secondary antibodies: Donkey anti-Chicken IgY (H+L), Alexa Fluor 488 (Invitrogen, A78948, 1:4000) and Donkey Anti-Rabbit IgG (H&L), Alexa Fluor 647 (Abcam, AB150075, 1:500) for 1 h at room temperature.

4. RT-qPCR

Reverse transcription was performed using SweScript All-in-One RT SuperMix for qPCR (One-Step gDNA Remover) (Servicebio, G3337) on a T20S PCR System (Hangzhou Langji Scientific Co., Ltd.) with the following program: 25°C for 5 min, 42°C for 30 min, and 85°C for 5 s. Quantitative PCR was conducted using 2×Universal Blue SYBR Green qPCR Master Mix (Servicebio, G3326) on a Bio-Rad CFX Connect real-time PCR system. The amplification program consisted of an initial denaturation at 95°C for 30 s, followed by 40 cycles of 95°C for 15 s and 60°C for 30 s. A melt-curve analysis was performed subsequently to confirm amplification specificity.

Primer	Sequence
GAPDH-F	CCTCGTCCCGTAGACAAAATG
GAPDH-R	TGAGGTCAATGAAGGGGTCGT
Lrp2-F	CCCGACTTTGAATCTGGTAGCA
Lrp2-R	CAACCCAGTCCACGGCTAATC

Ifnb1-F	AACTCCACCAGCAGACAGTG
Ifnb1-R	GGTACCTTTGCACCCTCCAG
Cxcl10-F	AAGCGTTTAGCCAAAAAAGGTC
Cxcl10-R	ACTGGGTAAAGGGGAGTGATGG
Il6-F	ACAACCACGGCCTTCCCTAC
Il6-R	GCACAACTCTTTTCTCATTTCCAC
Apoe-F	GTGCTGTTGGTCACATTGCTG
Apoe-R	CATCAGTGCCGTCAGTTCTTGT
Cx3cl1-F	CCGCGTTCTTCCATTTGTG
Cx3cl1-R	CACTGGGATTCGTGAGGTCAT
Irf1-F	CGGCTGGACTTGGACTTTCT
Irf1-R	GCCATTCACACAGGCCGATA
Tnf-F	AAATGGCAAATCGGCTGACG
Tnf-R	GTAGCCCACGTCGTAGCAAA
Il10-F	TAGACACCTTTGTCTTGGAGCTTA
Il10-R	CCTCTGGATACAGCTGCGAC
Arg1-F	TGGTCTCTCACATTGTACTCTGTTT
Arg1-R	AGATGTGCCCTCTGTCTTTTAG
Cd274-F	TCCTCGCCTACAGGTAAGT
Cd274-R	ACGTACAGGTCCTTTGGAGC
Hmgcr-F	AGCTTGCCCGAATTGTATGTG
Hmgcr-R	TCTGTTGTGAACCATGTGACTTC
Dhcr24-F	CTCTGGGTGCGAGTGAAGG
Dhcr24-R	TTCCCGGACCTGTTTCTGGAT
Abca1-F	GCTTGTTGGCCTCAGTTAAGG
Abca1-R	GTAGCTCAGGCGTACAGAGAT
Srebf2-F	GCAGCAACGGGACCATTCT
Srebf2-R	CCCCATGACTAAGTCCTTCAACT

5. Gene lists used for classical and basal signature scoring [1]

Classical	Basal
BTNL8	VGLL1
FAM3D	UCA1
PRR15L	S100A2
AGR3	LY6D
CTSE	SPRR3
LYZ	SPRR1B
TFF2	LEMD1
TFF1	KRT15
ANXA10	CTSV
LGALS4	DHRS9
PLA2G10	AREG
CEACAM6	CST6
VSIG2	SERPINB3
TSPAN8	KRT6A
ST6GALNAC1	SERPINB4
AGR2	FAM83A
TFF3	SCEL
CYP3A7	FGFBP1
MYO1A	KRT7
CLRN3	KRT17
KRT20	GPR87
CDH17	TNS4
SPINK4	SLC2A1
REG4	ANXA8L1

[1] Moffitt RA, Marayati R, Flate EL, Volmar KE, Loeza SG, Hoadley KA, et al. Virtual microdissection identifies distinct tumor- and stroma-specific subtypes of pancreatic ductal adenocarcinoma. Nat Genet. 2015;47(10):1168-78. Epub

2015/09/08. doi: 10.1038/ng.3398.

6. Signature scores for each tumor cell subpopulation

seurat_clusters	basal	classic
0	0.081703	0.240588
1	0.0456	0.109405
2	0.042885	0.312118
3	0.154798	0.137765
4	0.16705	0.04665
5	0.027967	0.270309
6	0.146868	0.191855
7	0.059287	0.231631
8	0.064063	0.070285
9	0.070777	0.168133
10	0.169816	0.016651
11	0.024993	0.314159
12	0.086598	0.061498
13	0.023571	0.030487
14	0.004247	0.013822

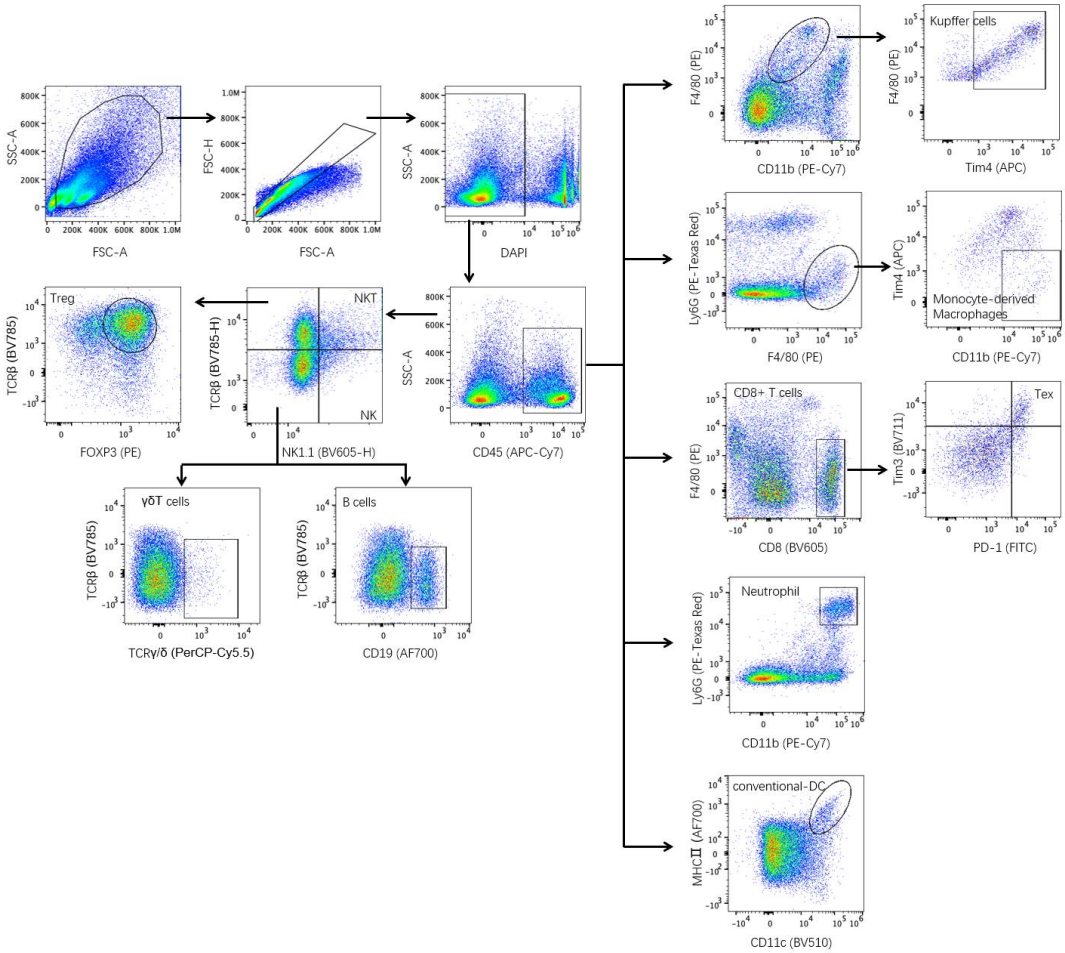

Supplementary Figure 1 Flow cytometry gating strategies. Single-cell suspensions were divided into two equal aliquots and stained separately using two antibody panels: A myeloid/Tex panel and an NK/Treg panel. $CD45^+$ immune cells were subsequently selected for downstream analysis. For the myeloid/Tex panel, immune subsets were identified using a sequential branching gating strategy. For the NK/Treg panel, $CD45^+$ cells were first subdivided into four major populations, followed by additional branching gates within the relevant quadrant to define specific lymphoid subsets.

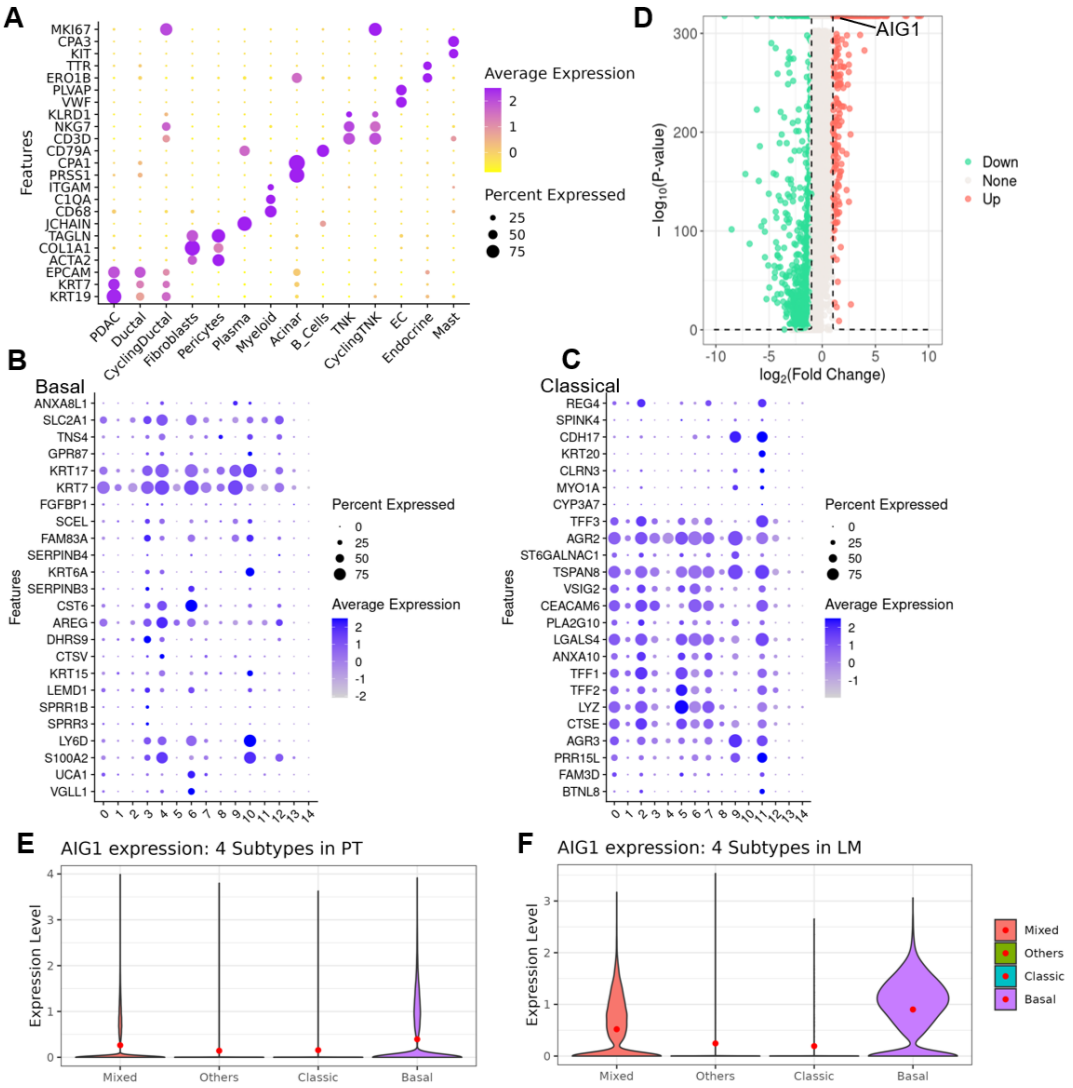

Supplementary Figure 2 A: Marker-based annotation of major cell populations in human pancreatic scRNA-seq datasets. B-C: Dot plot of basal and classical gene signatures across PDAC tumor cell subpopulations. Served as the reference for UCell scoring and subsequent cluster reannotation. D: Differential gene expression analysis between LM and PT tumor cells. AIG1 is present among the DEGs and shows a highly significant adjusted *p* value. (E-F) AIG1 expression across tumor cell subpopulations in PT and LM. AIG1 is relatively higher in basal-like tumor cells compared with other subpopulations. Non-parametric tests (Kruskal-Wallis for four-group comparison; Wilcoxon rank-sum for basal vs. classical) were used, with $P < 0.0001$.

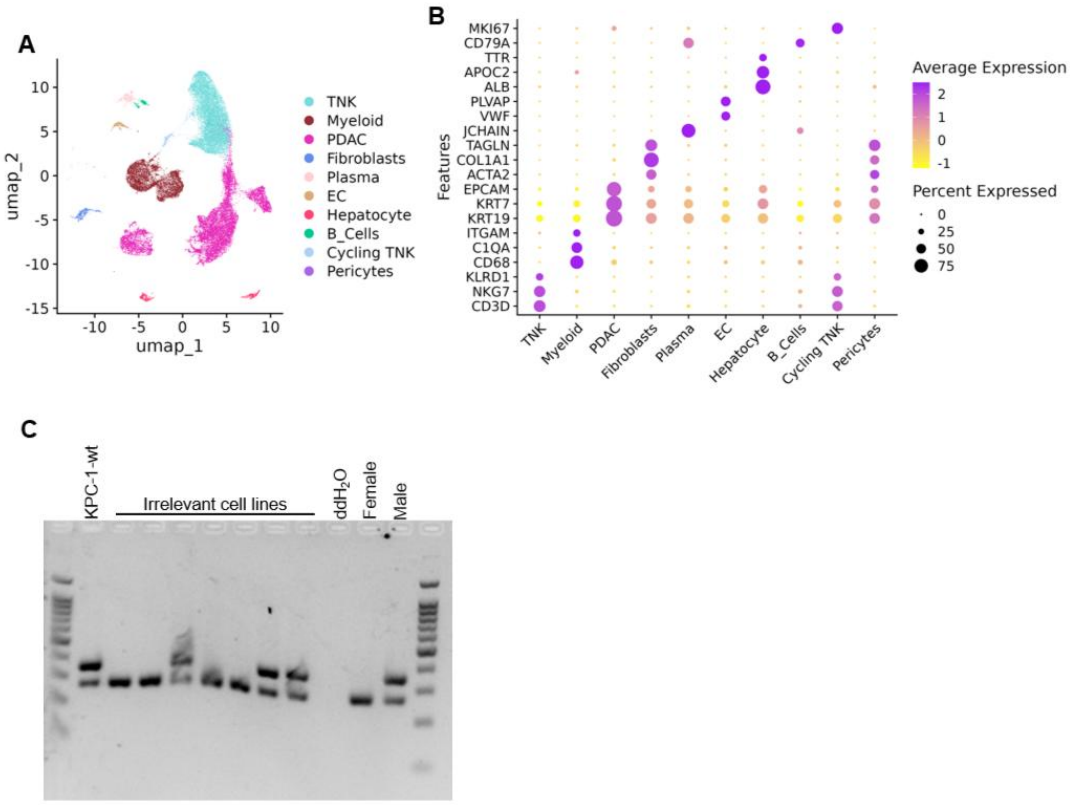

Supplementary Figure 3 (A) UMAP visualization of scRNA-seq from selected PDAC liver metastasis samples (*n* = 9), following reprocessing and unsupervised clustering. Major cell populations were annotated based on canonical marker genes. (B) DotPlot showing representative marker gene expression across annotated cell populations, confirming accurate cell-type identification. (C) PCR-based sex genotyping of KPC-1 cells. Genomic DNA extracted from KPC-1 cells was subjected to PCR amplification using primers specific for the sex chromosome marker gene. Agarose gel electrophoresis demonstrated the presence of the Y chromosome-specific band, confirming the male (XY) origin of KPC-1 cells. Male and female mouse genomic DNA were included as controls, respectively.

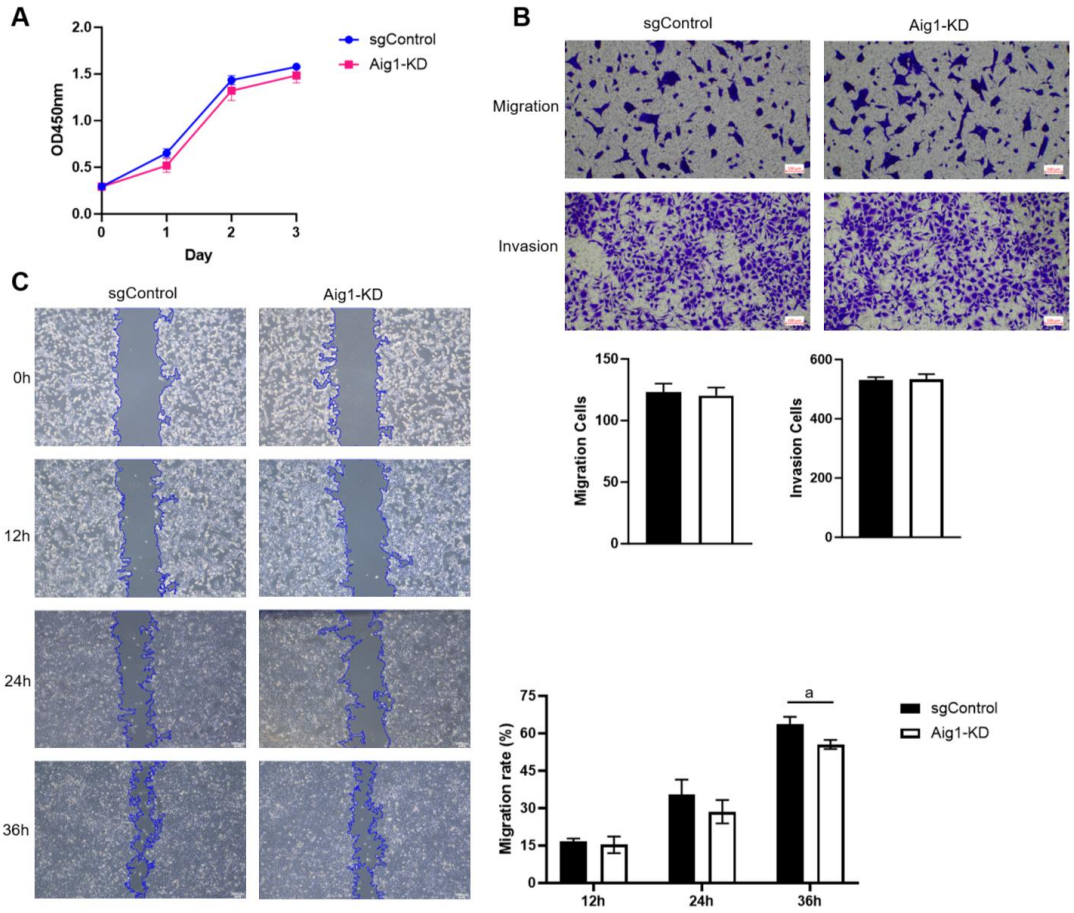

Supplementary Figure 4 In vitro proliferation, migration, and invasion assays of Aig1-KD *vs* gControl cells. (A) CCK-8 assay on days 0, 1, 2, and 3 post-seeding. Statistical analysis was performed using two-way ANOVA with multiple comparisons test. No significant differences were observed between groups at any time point (all ns). **(B)** Transwell migration and invasion assays (24 h). Statistical analysis was performed using unpaired *t*-tests. No significant differences in migration or invasion were observed between groups (both ns). **(C)** Wound-healing assay at 0, 12, 24, 36 h. Statistical analysis was performed using unpaired *t*-tests. $^{a}P < 0.05$ at 36 h; ns at 12 and 24 h. Data are presented as mean ± SD of three independent experiments.

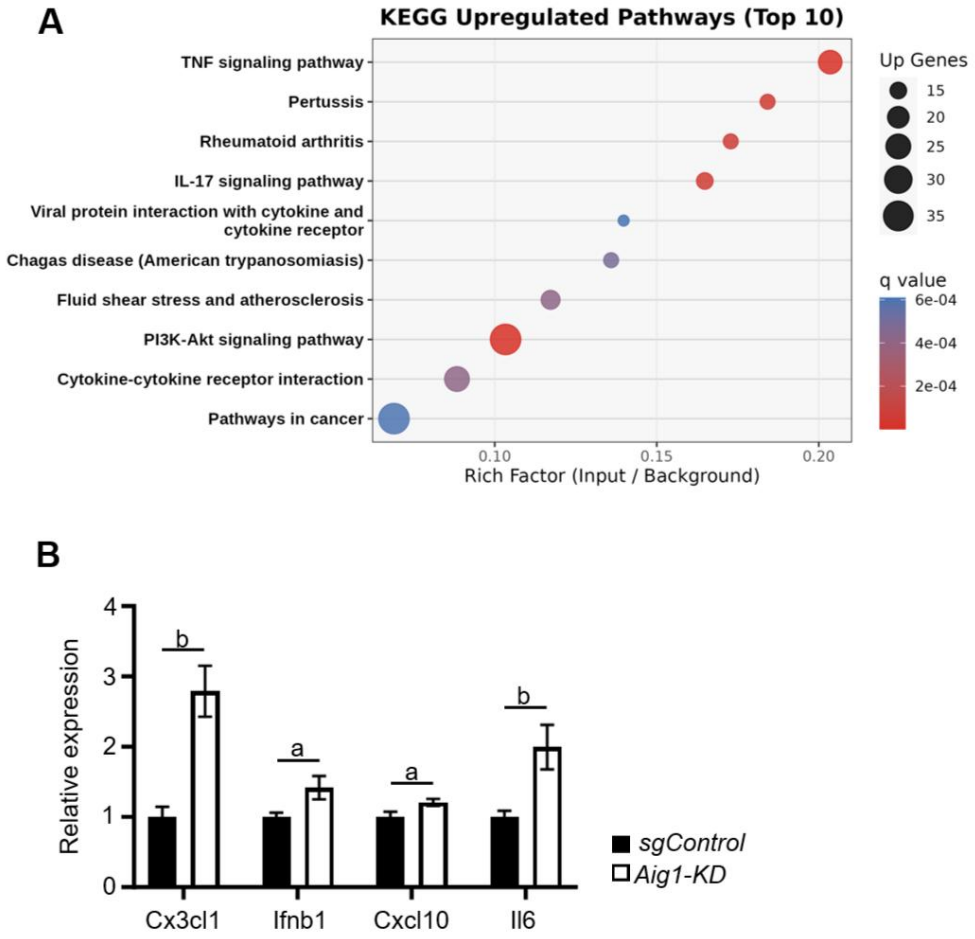

Supplementary Figure 5 *Aig1* knockdown promotes a pro-inflammatory transcriptional program. (A) KEGG enrichment analysis of upregulated genes. The q value shown in the plot represents the FDR-adjusted *p* value. **(B)** qPCR validation of inflammatory mediators (*Cx3cl1*, IFNB1, *Cxcl10*, and *Il6*) in sgControl and Aig1-KD cells. Data are presented as mean ± SD of three independent experiments. Statistical analysis was performed using unpaired *t*-tests. $^{a}P < 0.05$; $^{b}P < 0.01$

Supplementary Table 1 Information of all samples from public human single-cell databases

Disease State	n_GSE	GSE_list	n_patients	patient_list	cell counts
Donor	1	GSE229413	6 (6 donors, 11 sequencing runs)	GSM7162998_3829-EC, GSM7162999_3861-EC, GSM7163000_3862-EC, GSM7163001_4160-EC, GSM7163002_4161-EC, GSM7163003_4346-EC, GSM7163004_4347-EC, GSM7163007_4637-EC1, GSM7163008_4637-EC2, GSM7163009_4741-EC1, GSM7163010_4741-EC2	32555
Primary tumor	10	GSE154778, GSE156405, GSE194247, GSE202051, GSE205013, GSE211644, EGAS00001002543, PRJCA001063, phs001840.v1.p1, GSE155698	172	T1, T10, T2, T3, T4, T5, T6, T8, T9, SRR12467642, SRR12467643, SRR12467644, SRR12467645, SRR12467646, GEX_4, GEX_45_MM--ATTTGCTA, GEX_5, GEX_6, GEX_9, SRR19039304, SRR19039305, SRR19039306, SRR19039308, SRR19039309, SRR19039310, SRR19039311, SRR19039312, SRR19039313, SRR19039314, SRR19039315, SRR19039316, SRR19039317, SRR19039318, SRR19039319, SRR19039320, SRR19039321, SRR19039322, SRR19039323, SRR19039324,	543365

SRR19039325, SRR19039326, SRR19039327, SRR19039328,
SRR19039329, SRR19039330, SRR19039331, SRR19039332,
SRR19039333, SRR19039334, SRR19039335, SRR19039336,
SRR19039337, SRR19039338, SRR19039339, SRR19039342,
SRR19039343, SRR19039344, SRR19039345, SRR19039346,
SRR19039347, SRR19039348, SRR19039349, SRR19039350,
SRR19039351, SRR19039352, SRR19039353, SRR19039354,
SRR19039355, SRR19039365, SRR19039366, SRR19039367,
SRR19039368, SRR19039369, SRR19039370, SRR19039371,
SRR19039372, SRR19039373, SRR19039374, SRR19039375,
SRR19039376, SRR19039377, GSM6204111, GSM6204112,
GSM6204113, GSM6204114, GSM6204115, GSM6204116,
GSM6204117, GSM6204118, GSM6204120, GSM6204121,
GSM6204122, GSM6204123, GSM6204127, GSM6204128,
GSM6204130, GSM6204131, GSM6204134, SRR18025515,
SRR18045262, SRR18045263, SRR18045264, SRR18045265,
SRR18045266, SRR18045267, SRR18045268, SRR21152729,

SRR21152730, SRR21152731, SRR21152732, SRR21152733, SRR21152734, 100070, 85948, 87235, 87784, 91412, 91610, 91706, 94930, 95092, 95373, 96460, 97727, G9903, new_CRR034499, new_CRR034500, new_CRR034501, new_CRR034503, new_CRR034504, new_CRR034505, new_CRR034506, new_CRR034507, new_CRR034509, new_CRR034511, new_CRR034512, new_CRR034513, new_CRR034516, new_CRR034517, new_CRR034518, new_CRR034519, new_CRR241798, new_CRR241799, new_CRR241800, new_CRR241801, new_CRR241802, new_CRR241803, new_CRR241804, new_CRR241805, SRR9274536, SRR9274537, SRR9274538, SRR9274539, SRR9274540, SRR9274542, SRR9274544, SRR12461530, SRR12461533, SRR12461536, SRR12461538, SRR12461548, SRR12507930, SRR12507931, SRR12507934, SRR12507935, SRR12507938, SRR12507939, SRR12508148, SRR12532883, SRR12532884, SRR12532885, SRR12532886

Liver metastatic lesion	4	GSE154778, GSE156405, GSE158356, GSE205013	21	Y00006_HT77VBCXY_AACCGTAA, Y00013_HW7W7AFXX_TTGGCATA, Y00014_HW7W7AFXX_TGAAGTAC, Y00016_HW7W7AFXX_GTTGCAGC, Y00019_H5HVVBGX5_GATCTCAG, Y00027_H5HVVBGX5_ACGACATT, SRR12467648, LiverMetA, LiverMetB, LiverMetC, LiverMetE, GSM6204109, GSM6204110, GSM6204119, GSM6204124, GSM6204125, GSM6204126, GSM6204129, GSM6204132, GSM6204133, GSM6204135	52292

Supplementary Table 2 Information of public single-cell sequencing samples from PDAC liver metastases with known sex

Database ID	Patient ID	Gender	Age	Treatment before tissue collection	
GSE205013	P01	M	78	N	
	P02	M	74	N	
	P11	F	73	N	
	P16	F	69	N	
	P17	M	64	Y	exclude
	P18	M	75	N	
	P21	M	69	N	
	P24	F	65	N	
	P25	M	48	N	
	P27	F	72	N	

Supplementary Table 3 In silico off-target prediction of Aig1 sgRNA by CRISPOR and RNA-seq validation

Rank	Gene	Genomic region	Mismatch Count	CFD score	RNA-seq log2FC	RNA-seq adjusted p value
1	Macrod2	intron	3	0.5625	0.266077	0.203327
2	Kcnq3	intron	3	0.446875	None	None
3	Gabrb3	intron	3	0.254545	None	None
4	Adcy9	exon	3	0.207692	0.479735	3.76E-07
5	Padi1	intron	3	0.192837	-0.99788	0.202594
6	Armc4	intron	3	0.185759	None	None
7	Csmd2	intron	3	0.181818	-1.58774	0.1187
8	Nr1i2	intron	3	0.116354	None	None
9	Bbs9	intron	3	0.113749	-0.14949	0.332525
10	Hnrnpc	intron	3	0.108791	-0.09984	0.127989